Rapid sulfuric acid–dimethylamine nucleation enhanced by nitric acid in polluted regions

Ling Liu[a], Fangqun Yu[b], Lin Du[c], Zhi Yang[a], Joseph S. Francisco[d,e,1], and Xiuhui Zhang[a,1]

[a]Key Laboratory of Cluster Science, Ministry of Education of China, School of Chemistry and Chemical Engineering, Beijing Institute of Technology, Beijing 100081, China; [b]Atmospheric Sciences Research Center, University at Albany, Albany, NY 12203; [c]Environment Research Institute, Shandong University, Qingdao 266237, China; [d]Department of Earth and Environmental Sciences, University of Pennsylvania, Philadelphia, PA 19104; and [e]Department of Chemistry, University of Pennsylvania, Philadelphia, PA 19104

Edited by Mark Thiemens, University of California, San Diego, La Jolla, CA, and approved July 12, 2021 (received for review May 4, 2021)

Recent research [Wang *et al.*, *Nature* 581, 184–189 (2020)] indicates nitric acid (NA) can participate in sulfuric acid (SA)–ammonia (NH_3) nucleation in the clean and cold upper free troposphere, whereas NA exhibits no obvious effects at the boundary layer with relatively high temperatures. Herein, considering that an SA–dimethylamine (DMA) nucleation mechanism was detected in megacities [Yao *et al.*, *Science* 361, 278–281 (2018)], the roles of NA in SA-DMA nucleation are investigated. Different from SA-NH_3 nucleation, we found that NA can enhance SA-DMA–based particle formation rates in the polluted atmospheric boundary layer, such as Beijing in winter, with the enhancement up to 80-fold. Moreover, we found that NA can promote the number concentrations of nucleation clusters (up to 27-fold) and contribute 76% of cluster formation pathways at 280 K. The enhancements on particle formation by NA are critical for particulate pollution in the polluted boundary layer with relatively high NA and DMA concentrations.

atmospheric aerosol | nitric acid | nucleation | sulfuric acid–dimethylamine | polluted regions

New particle formation (NPF) can contribute to more than half of the atmospheric aerosols in terms of their number abundance, which can have adverse impacts on the environment and human health. New particles can also lead to the production of larger, longer-lived particles that can then serve as cloud condensation nuclei and have further profound impacts on the climate (1, 2). In the NPF process, nucleation is viewed as the key stage (1), in which sulfuric acid (SA) is regarded as the dominant nucleation precursor due to its extremely low volatility and high acidity (3, 4). In addition, a number of species have been identified to participate in the atmospheric NPF. However, the prevailing nucleation mechanisms cannot fully elucidate the complex nucleation in the polluted regions (5–7). Hence, there are still unidentified nucleation species or mechanisms responsible for NPF in the atmosphere.

Nitric acid (NA), an important atmospheric inorganic acid, can be generated from photochemical smog, combustion of fossil fuels or biomass, and many other natural and anthropogenic sources (8). It is one of the most abundant pollutants in the atmosphere, the concentration of which can reach as high as 10^{11} molecules $\cdot$ cm^{-3} in polluted areas (9–11). However, its role in the NPF has always been neglected. In the year 2020, Wang et al. performed a CLOUD (Cosmics Leaving OUtdoor Droplets) chamber experiment (12) to investigate the role of NA in the nucleation process of SA-NH_3 particles. Their results indicate that NA can participate in the SA-NH_3 nucleation in the relatively clean and cold upper free troposphere, especially in agricultural areas where NH_3 is abundant (12, 13). However, it has a negligible effect on SA-NH_3 nucleation at the atmospheric boundary layer due to the relatively high temperature. The role of NA in the polluted atmospheric boundary layer was also not considered, although there is more NA in the polluted areas than relatively clean areas. Thus, it is urgent to give the role of NA in tropospheric nucleation a comprehensive perspective. Although field measurements showed that the NPF process in certain areas may be dominated by nucleation involving SA and dimethylamine (DMA) (14), there were still many kinds of unidentified species. The role of abundant NA (15) in SA-DMA nucleation cannot be eliminated because of the nitrate reagent ions used in this measurement protocol, which may mask the signal of clusters involving NA. Thus, to elucidate the role of NA in polluted regions, it is important to investigate the effects of NA on SA-DMA nucleation, the results of which could likely help to further explain frequent NPF events in the polluted atmospheric boundary layer.

Herein, we studied the roles of NA in the SA-DMA nucleation process in the atmospheric boundary layer using Density Functional Theory combined with Atmospheric Clusters Dynamic Code (ACDC) (16, 17). The enhancement degrees by NA on particle formation rates and number concentrations of clusters in the SA-DMA system are predicted under different atmospheric conditions related to the boundary layer. Finally, the SA-DMA-NA rapid nucleation mechanism is proposed based on our theoretical simulation results.

Results and Discussion

Particle Formation Rates Enhanced by NA. NA can form clusters (*SI Appendix*, Fig. S1) with SA and DMA by relatively strong intermolecular hydrogen bonds as indicated by topological analysis (*SI Appendix*, section S1 and Table S1) according to the atoms in molecules theory (18) and even proton-transfer interaction as shown by color-filled localized orbital locator (19) maps (*SI Appendix*, Fig. S2) and the proton-transfer parameter (20, 21) (*SI Appendix*, section

Significance

Nucleation of atmospheric aerosol particles can contribute to nearly half of global cloud condensation nuclei. Nitric acid (NA) is one of the most abundant atmospheric pollutants. A recent study suggested that NA is likely to participate in the sulfuric acid–ammonia nucleation only in the clean and cold upper free troposphere, but its role in the polluted atmospheric boundary layer was not considered. Herein, we found that NA can extensively participate in and significantly enhance the predominant sulfuric acid–dimethylamine nucleation in the polluted boundary layer. Thus, controls on the emissions of nitrogen pollutants are likely significant for the reduction of particulate pollution, especially in the polluted regions.

Author contributions: J.S.F. and X.Z. designed research; L.L., F.Y., J.S.F., and X.Z. performed research; L.L., F.Y., L.D., Z.Y., J.S.F., and X.Z. analyzed data; and L.L., F.Y., L.D., Z.Y., J.S.F., and X.Z. wrote the paper.

The authors declare no competing interest.

This article is a PNAS Direct Submission.

[1]To whom correspondence may be addressed. Email: zhangxiuhui@bit.edu.cn or frjoseph@sas.upenn.edu.

This article contains supporting information online at https://www.pnas.org/lookup/suppl/doi:10.1073/pnas.2108384118/-/DCSupplemental.

Published August 27, 2021.

S1 and Table S2). Moreover, clusters containing NA, such as $(SA)_1 \cdot (DMA)_2 \cdot (NA)_1$, $(SA)_1 \cdot (DMA)_3 \cdot (NA)_2$, and $(SA)_2 \cdot (DMA)_3 \cdot (NA)_1$, can continue to grow to larger clusters with mobility diameters larger than 1.5 nm due to their collision rates being higher than their corresponding evaporation rates (*SI Appendix*, section S2 and Fig. S3). This indicates that these clusters involving NA can potentially participate in the SA-DMA nucleation process. Thus, it is necessary to further study the effects of NA on the particle formation rates of the SA-DMA nucleation system.

The particle formation rate (J) was studied to understand the detailed role of NA in the SA-DMA particle formation process. As shown in Fig. 1*A*, the simulated J of the SA-DMA system, which is proved to be the predominant nucleation mechanism in Shanghai (14), by ACDC (black dashed lines) in the present study is close to the measured J in NPF events (12) in Shanghai (gray squares), China. This indicates the reliability of the ACDC simulation on the SA-DMA system. At the predicted [DMA] of 1.25×10^8 molecules $\cdot$ cm^{-3} in NPF events in Shanghai, the simulated J at [NA] in the range of 1.0×10^{10} molecules $\cdot$ cm^{-3} (magenta line) to 1.0×10^{11} molecules $\cdot$ cm^{-3} (green line) can be comparable with some of the measured J (gray squares) and can be higher than the simulated J of the pure SA-DMA system (black dashed line) by up to 1.5-fold at [SA] of 5.0×10^6 molecules $\cdot$ cm^{-3} [approximate to the reported SA concentration in Shanghai (12)] and 5.0-fold at [SA] of 1.0×10^6 molecules $\cdot$ cm^{-3}. Thus, NA can potentially participate in SA-DMA nucleation at the observed [DMA] of 1.25×10^8 molecules $\cdot$ cm^{-3} in Shanghai. When [DMA] increases from 1.25×10^8 molecules $\cdot$ cm^{-3} to 1.0×10^9 molecules $\cdot$ cm^{-3}, the simulated J of the SA-DMA system by ACDC (black line in *SI Appendix*, Fig. S4) can increase to be comparable with most of the relatively high measured J in Shanghai (gray squares in *SI Appendix*, Fig. S4). The simulated J can further increase gradually with the increase of [NA] at [DMA] of 1.0×10^9 molecules $\cdot$ cm^{-3}. At [DMA] of 1.0×10^9 molecules $\cdot$ cm^{-3} and [SA] of 5.0×10^6 molecules $\cdot$ cm^{-3}, the J at [NA] of 1.0×10^{10} molecules $\cdot$ cm^{-3} and 1.0×10^{11} molecules $\cdot$ cm^{-3} can be about 1.7-fold (red line in *SI Appendix*, Fig. S4) and 15.6-fold (blue line in *SI Appendix*, Fig. S4) higher than the corresponding J of SA-DMA system (black line in *SI Appendix*, Fig. S4), respectively. Therefore, it is possible that NA participates in SA-DMA nucleation in Shanghai when there is heavy traffic, resulting in high [NA] and [DMA] (15). SA-DMA-NA

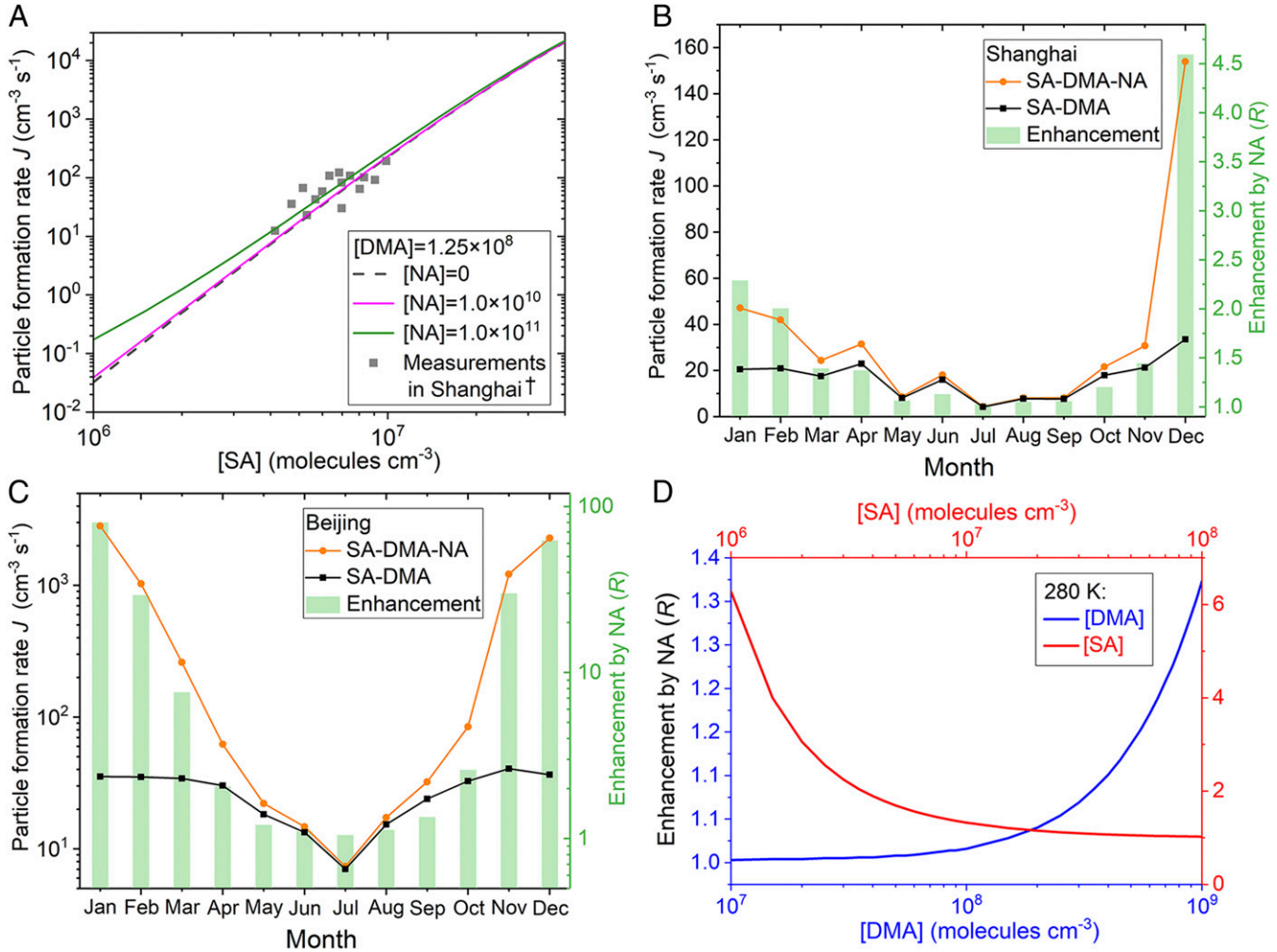

Fig. 1. (*A*) Particle formation rates (J, cm$^{-3} \cdot$ s^{-1}) as a function of [SA] and 280 K. Gray squares represent the measured particle formation rates in Shanghai, China†. Lines represent the simulated J by ACDC at the corresponding concentrations of nucleation precursors shown in the graph legend. Simulated particle formation rates of the SA-DMA-NA (orange circles) and SA-DMA (black squares) systems and the enhancement by NA ($R = J_{SA\text{-}DMA\text{-}NA}/J_{SA\text{-}DMA}$) in different months depending on the corresponding temperature and DMA concentration in (*B*) Shanghai, China, and (*C*) Beijing, China. [SA] = 5.0×10^6 molecules $\cdot$ cm^{-3} and [NA] = 1.0×10^{10} molecules $\cdot$ cm^{-3}. (*D*) Enhancement on particle formation rate by NA ($R = J_{SA\text{-}DMA\text{-}NA}/J_{SA\text{-}DMA}$) as a function of the [DMA] (blue line, [SA] = 1.0×10^7 molecules $\cdot$ cm^{-3}, [NA] = 1.0×10^{10} molecules $\cdot$ cm^{-3}) and [SA] (red line, [DMA] = 1.0×10^9 molecules $\cdot$ cm^{-3}, [NA] = 1.0×10^{10} molecules $\cdot$ cm^{-3}) at 280 K. †Yao et al. (14).

clusters were not captured in previous field measurements in Shanghai (14), possibly because nitrate reagent ions were used in the mass spectrometer measurement protocol, which masked the signal of clusters involving NA. If there are suitable reagent ions for the measurement of NO_3^-, the SA-DMA-NA clusters may potentially be measured in field experiments.

To understand the detailed influence of NA on SA-DMA nucleation under actual atmospheric conditions, J and enhancement by NA (R) were studied under the corresponding measured temperatures from the NASA Langley Research Center POWER Project (22) and DMA concentrations associated with predictions by the global chemistry-transport model of GEOS-Chem (23) in different months in six typical cities. The corresponding [DMA] and temperatures in different months of the studied cities are shown in *SI Appendix*, Table S3. The simulated particle formation rates (Fig. 1*B*) are almost at the same order of magnitude as the measurements in Shanghai (12), among which the J in December is about one order of magnitude higher than those in other months because of the low temperature and high [DMA] in December (*SI Appendix*, Table S3). The participation of NA in SA-DMA nucleation can lead to J being up to 4.6 times higher in cold and polluted December. Moreover, the enhancement of R by NA is relatively significant and can be up to 80-fold in January in Beijing (Fig. 1*C*). The role of NA in other polluted and less polluted areas has also been studied (*SI Appendix*, Fig. S5). The simulated particle formation rates in Värriö, Finland, do not change significantly with seasonal variations, which is similar with the variation trend by measurements (24, 25). The R is around one all year round in Värriö. Therefore, the enhancement by NA on NPF is not obvious in less polluted areas and can be significant in cold and polluted regions.

The enhancements on particle formation rate by NA at different concentrations of nucleation precursors are further explored. As shown in Fig. 1*D*, the enhancement on the SA-DMA particle formation rate by NA ($R = J_{\text{SA-DMA-NA}}/J_{\text{SA-DMA}}$) at the common temperature of the atmospheric boundary layer (280 K) can be up to 6.3-fold at relatively high [DMA] (1.0×10^9 molecules $\cdot$ cm^{-3}), medium [NA] (1.0×10^{10} molecules $\cdot$ cm^{-3}), and low [SA] (1.0×10^6 molecules $\cdot$ cm^{-3}). Furthermore, the enhancement on J by NA can increase with decreasing temperature and can be up to 3.7×10^6-fold at 240 K (*SI Appendix*, Fig. S6). Though sulfur-containing species can be emitted to the atmosphere from natural sources, and the changes in its anthropogenic emissions may change the ambient particles and further influence the survival process of new particles, the role of NA in the NPF process may likely become significant to some extent with the effective control of the emissions of sulfur-containing pollutants. Therefore, in the regions far away from the emission source of sulfur-containing pollutants, the frequent and intense NPF can also occur with the enhancement of NA, especially at relatively low temperatures, high [DMA], and high [NA], such as in the polluted atmospheric boundary layer in urban areas with heavy traffic or near sources of nitrogen-containing gas and far away from industrial sources of sulfur-containing gas, especially in winter.

Previously, the CLOUD experiment revealed that NA can enhance SA-NH_3 nucleation in the cold and clean upper troposphere with relatively low [SA] (12). The J of the SA-NH_3-NA and SA-DMA-NA systems are compared (*SI Appendix*, Fig. S7) to better understand the role of NA in the NPF process. The simulated J of the SA-DMA-NA system is about three orders of magnitude higher than the simulated J of the SA-NH_3-NA system under the corresponding CLOUD experimental conditions (12). The Gibbs free energies of formation (ΔG) for SA-DMA-NA clusters are more negative than those for SA-NH_3-NA clusters (*SI Appendix*, Tables S4 and S5), which is caused by the stabilizing effects of both DMA and NA. The more negative ΔG leads to the stability of SA-DMA-NA clusters being stronger than that of SA-NH_3-NA clusters, and thus the J of the SA-DMA-NA system is higher than that of the SA-NH_3-NA system. Therefore, NA not only participates in SA-NH_3 nucleation in the clean and cold upper troposphere but can also participate in SA-DMA nucleation more rapidly in the polluted atmospheric boundary layer with relatively high temperatures.

Nucleation Cluster Concentrations Enhanced by NA. Though the particle formation rate is always studied by the experiments or filed measurements that can reflect the kinetic characteristics of the particle formation process, the number concentration of particles is a more relevant variable for many applications (26, 27). Thus, to study the influence of NA on the concentrations of SA-DMA clusters, the cluster concentrations of the SA-DMA-NA system were explored at different temperatures (280 K and 260 K) and different nucleation precursor concentrations ([NA], [SA], and [DMA]) relevant to the atmospheric boundary layer.

Under the concentration conditions of SA and DMA corresponding to the relatively strong enhancement of R by NA ([SA] = 5.0×10^6 molecules $\cdot$ cm^{-3} and [DMA] = 1.0×10^9 molecules $\cdot$ cm^{-3}), the concentrations of clusters with different numbers of molecules at the common temperature in the atmospheric boundary layer of 280 K were studied. As shown in Fig. 2*A*, it can be discerned that concentrations of clusters with different numbers of molecules of the SA-DMA-NA system (orange, green, and blue histograms) are all higher than those of clusters with the same number of molecules of the SA-DMA system (gray histograms) at different [NA]. Thus, the participation of NA can enhance the number concentrations of clusters at different [NA] in the formation of SA-DMA clusters. The detailed enhancement on cluster concentrations by NA at different [NA] was further explored at the same concentrations of nucleation precursors and 280 K. As shown in Fig. 2*B*, the enhancements on concentrations of different kinds of clusters (with different numbers of molecules) in the SA-DMA system by NA are positively correlated with [NA] and can be up to 27-fold at [NA] of 1.0×10^{11} molecules $\cdot$ cm^{-3}. For the largest studied clusters with six molecules and the mobility diameter larger than 1.5 nm, the enhancement on their concentrations by NA can be about eightfold at [NA] of 1.0×10^{11} molecules $\cdot$ cm^{-3}. Furthermore, the concentrations of clusters and the enhancement of cluster concentration by NA at 280 K at different [DMA] and [SA] are illustrated in *SI Appendix*, Fig. S8. It can be seen that the participation of NA can enhance the number concentrations of clusters in the SA-DMA system at different [SA] and [DMA], and the enhancement by NA can be particularly significant at relatively low [SA] and high [DMA].

Furthermore, at different concentrations of nucleation precursors, the cluster concentrations and the concentration enhancements by NA at 260 K are all higher than those at 280 K, and the enhancement at 260 K can be up to 354-fold (*SI Appendix*, Fig. S9). For the largest studied clusters with six molecules and the mobility diameter larger than 1.5 nm, the enhancement on their concentrations of by NA can be 176-fold at [NA] of 1.0×10^{11} molecules $\cdot$ cm^{-3} and 260 K. The enhancement on cluster concentration by NA can increase as temperature decreases. Thus, it can be expected that the participation of NA in SA-DMA nucleation can likely enhance the number concentration of particulates significantly in the atmospheric boundary layer of cold and polluted areas with relatively high [NA] and [DMA].

Nucleation Cluster Formation Mechanisms Involving NA. To understand the mechanism whereby NA influences the formation of SA-DMA clusters in the atmospheric boundary layer, the cluster formation mechanism of the SA-DMA-NA system was studied at relevant nucleation precursor concentrations and temperatures. At [SA] of 5.0×10^6 molecules $\cdot$ cm^{-3} and [DMA] of 1.0×10^9 molecules $\cdot$ cm^{-3} corresponding to relatively strong enhancement

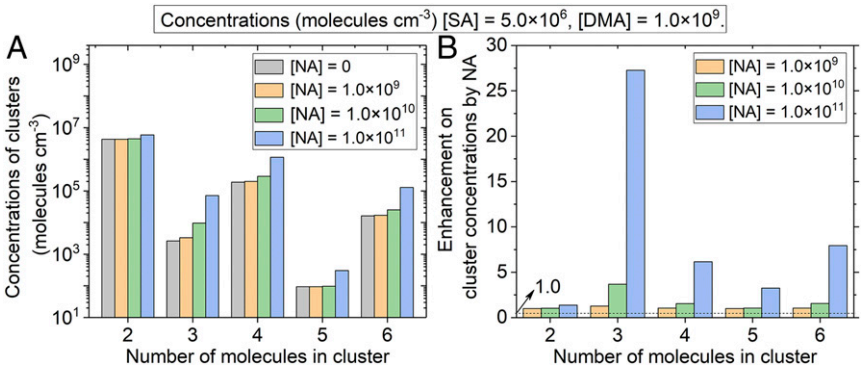

Fig. 2. (*A*) Concentrations (molecules · cm^{-3}) of clusters with different numbers of molecules for the SA-DMA-NA system and SA-DMA system, and (*B*) enhancement on concentrations of clusters with different numbers of molecules in the SA-DMA system by NA at different [NA] and 280 K.

of particle formation rates and cluster concentrations by NA, Fig. 3 shows the cluster formation pathway at different [NA] and different temperatures (280 K and 260 K). The $(SA)_3{\cdot}(DMA)_3$, $(SA)_2{\cdot}(DMA)_2$, $(SA)_1{\cdot}(DMA)_3{\cdot}(NA)_2$, and $(SA)_1{\cdot}(DMA)_2{\cdot}(NA)_1$, $(SA)_2{\cdot}(DMA)_3{\cdot}(NA)_1$ clusters can continue growing to or larger than the boundary clusters [$(SA)_4{\cdot}(DMA)_3$, $(SA)_4{\cdot}(DMA)_4$, $(SA)_3{\cdot}(DMA)_4{\cdot}(NA)_1$, $(SA)_2{\cdot}(DMA)_4{\cdot}(NA)_2$, and $(SA)_1{\cdot}(DMA)_4{\cdot}(NA)_3$]. The formation of the boundary clusters or larger clusters can contribute to the sum of particle formation rates. It is discernable that NA can participate in the cluster formation process.

At 280 K, the contribution of NA to the main cluster formation pathway increases from 0% to 76% (38% + 29% + 9%) with [NA] increasing from 1.0 × 10^9 molecules · cm^{-3} to 1.0 × 10^{11} molecules · cm^{-3} (Fig. 3). When [NA] increases up to 1.0 × 10^{11} molecules · cm^{-3}, clusters involving two molecules of NA, $(SA)_1{\cdot}(DMA)_3{\cdot}(NA)_2$, can also continue growing in addition to clusters involving one molecule of NA, $(SA)_1{\cdot}(DMA)_2{\cdot}(NA)_1$ and $(SA)_2{\cdot}(DMA)_3{\cdot}(NA)_1$. Therefore, not only can the contribution of NA to the main cluster formation pathway increase with the increase of [NA] but the number of NA molecules contained in clusters [$(SA)_1{\cdot}(DMA)_2{\cdot}(NA)_1$, $(SA)_2{\cdot}(DMA)_3{\cdot}(NA)_1$, and $(SA)_1{\cdot}(DMA)_3{\cdot}(NA)_2$] that can contribute to cluster growth can also be positively correlated with [NA]. The contributions of cluster formation pathways involving NA can increase with decreasing temperature, up to 83% (45% + 31% + 7%) at [NA] of 1.0 × 10^{10} molecules · cm^{-3} and 260 K (Fig. 3).

SI Appendix, Fig. S10 also shows the main cluster formation pathway at different [DMA] and [SA]. The contribution of NA to the main cluster formation pathway has a negative correlation with [SA] and a positive correlation with [DMA]. Therefore, NA not only participates in the SA-NH_3 nucleation process in the clean and cold upper troposphere (12) but can also extensively participate in the SA-DMA nucleation process and significantly contribute to the total cluster formation pathways in the polluted atmospheric boundary layer with high [DMA] and [NA] and low [SA] (Fig. 4), such as in megacities with heavy traffic and far away from emission sources of sulfur-containing pollutants. Moreover, the contributions can be more significant at lower temperatures, such as in winter.

Conclusion

We found that NA can significantly enhance SA-DMA cluster formation rates, especially in cold polluted areas, such as Beijing in winter. NA can also enhance the number concentration of

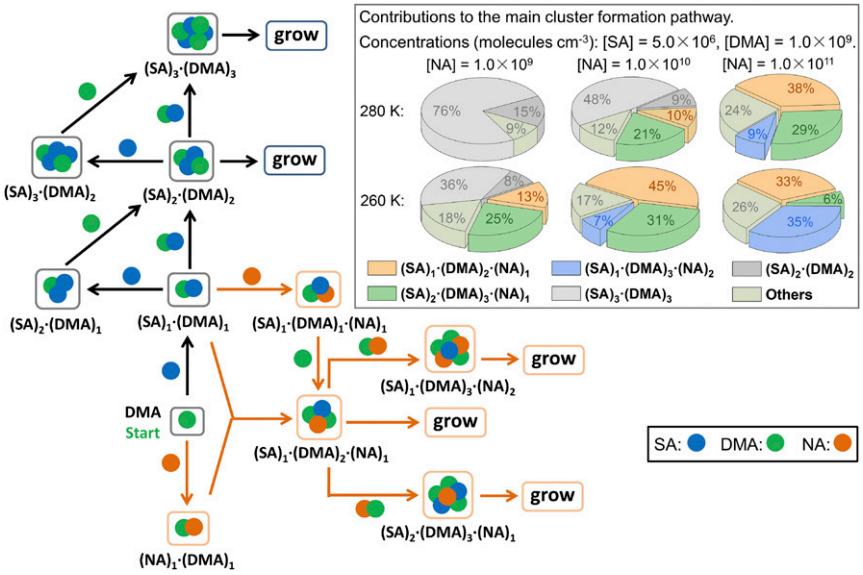

Fig. 3. Cluster formation pathways at different concentrations of NA at 280 K and 260 K. The contributions of different cluster formation pathways to the main cluster formation pathway are shown in the pie charts. Black and orange arrows indicate the pathways of pure SA-DMA cluster formation and SA-DMA-NA cluster formation, respectively.

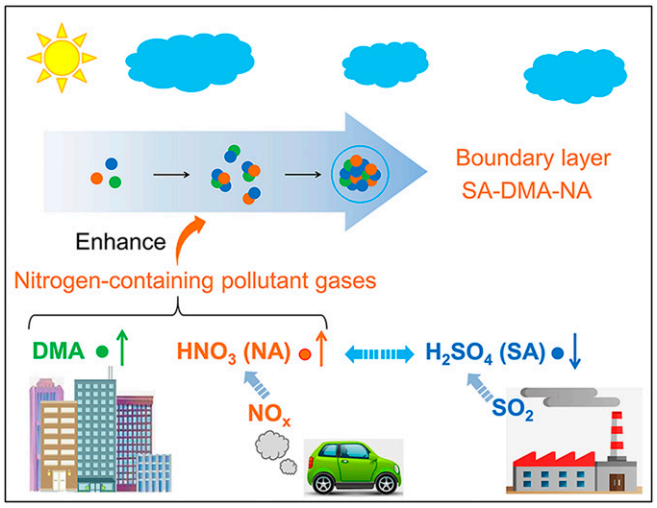

Fig. 4. Influence mechanisms of NA on SA-DMA–based cluster formation in the polluted boundary layer.

clusters and participate extensively in SA-DMA nucleation in the polluted atmospheric boundary layer with abundant NA and DMA. This enhancement mechanism can provide theoretical insights to explain the frequent occurrence of NPF events in the polluted boundary layer. Of particular note, the present study indicates that the control on emissions of nitrogen-containing pollutants (such as emissions from automobile exhausts and industry) can help to further reduce particulate pollution in the context of continuous emission controls of sulfur-containing pollutants to some extent.

Methods

To identify the structure with the lowest energy for each studied cluster, the ABCluster (28, 29) program was used to systematically generate initial cluster structures. All the molecules in the ABCluster program were described by the CHARMM36 force field (30). First, the 1,000 structures with relatively low energy were retrieved form ABCluster. Second, the PM7 semiempirical method (31) by MOPAC2016 (32) was used for optimization of these 1,000 structures. Third, up to 100 structures with low energies among the 1,000 structures were selected to be optimized at the M06-2X/6-31+G* level of theory (33, 34). Finally, the M06-2X/6–311++G(3df,3pd) (35) level of theory was chosen to reoptimize the 10 relatively stable structures among the 100 structures based on the excellent performance of this level of theory to calculate the properties of atmospherically relevant clusters (33, 36–40). Vibrational frequencies were calculated for the most stable structures of the studied clusters. All quantum chemistry calculations were carried out with the Gaussian 09 package (41). Furthermore, given that the DLPNO-CCSD(T)/aug-cc-pVTZ level of theory is a good compromise between cost and efficiency to calculate the binding energy of clusters with high accuracy (42, 43), single-point energy calculations were undertaken at the DLPNO-CCSD(T)/aug-cc-pVTZ (44–46) level of theory using the ORCA program (47). The corresponding ΔG of formation at the DLPNO-CCSD(T)/aug-cc-pVTZ//M06-2X/6–311++G(3df,3pd) level for the studied clusters are listed in *SI Appendix*, Table S6.

Cluster formation rates and mechanisms were simulated by the ACDC model, which generates birth–death equations for clusters and explicitly solves the time development of cluster concentrations by numerical integration using the ode15s solver in MATLAB (48). Both the outside source term of nucleation precursors and the sink term of clusters corresponding to the coagulation onto preexisting larger particles are considered in the ACDC model. Although the DLPNO-CCSD(T)/aug-cc-pVTZ can provide more accurate energies than RI-CC2/aug-cc-pV(T+d)Z (43, 46, 49), the simulated SA dimer concentrations (50) and particle formation rates of SA-DMA system (*SI Appendix*, Fig. S11) by the combination of ACDC and DLPNO-CCSD(T)/aug-cc-pVTZ both are approximately one order of magnitude lower than the present available field-measured results, such as in Shanghai (14). However, the simulated SA dimer concentrations (50) by the combination of ACDC and RI-CC2/aug-cc-pV(T+d)Z are in good agreement with the field measured results in Shanghai (14). Furthermore, the particle formation rates of the SA-DMA system predicted by the combination of ACDC and RI-CC2/aug-cc-pV(T+d)Z are in good agreement with both of the field-measured results in Shanghai (Fig. 1*A*) and the experimental results of the CLOUD chamber (51, 52). These agreements may be due to a random cancellation of errors, which is not within the scope of this study but should be revealed in forthcoming studies. Hence, we simulate the SA-DMA-NA clustering process at the RI-CC2/aug-cc-pV(T+d)Z level of theory to predict the experimental results.

The studied clusters are $(SA)_x{\cdot}(DMA)_y{\cdot}(NA)_z$, where $0 \le y \le (x + z) \le 3$. The temperatures used herein, 280 K and 260 K, represent the common range of the atmospheric boundary later. The concentrations of SA, DMA, and NA are in the common atmospheric concentration ranges of 1.0×10^6 to 1.0×10^8 molecules $\cdot$ cm^{-3} (14, 53, 54), 1.0×10^7 to 1.0×10^9 molecules $\cdot$ cm^{-3} (15), and 1.0×10^9 to 1.0×10^{11} molecules $\cdot$ cm^{-3} (55–61), respectively. Although the atmospheric water concentration is typically 8 to 10 orders of magnitude higher than those of other nucleation precursors (62), previous studies have found that the hydrogen bond interaction between water molecules and the acid (e.g., SA) or base (e.g., DMA) is weaker than that between acid and base molecules, and the influence of water on the clustering process (e.g., SA-DMA) is not significant (63–65). Given that both of SA and NA are relatively strong acids and DMA is a relatively strong base, it is expected that the SA-DMA-NA clustering process is not significantly affected by hydration. Hence, water molecules are not considered in the present study.

Data Availability. All data are available in the article and/or *SI Appendix*.

ACKNOWLEDGMENTS. X.Z. and L.D. are indebted to the National Natural Science Foundation of China (Grants 21976015 and 91644214). L.L. thanks the China Postdoctoral Science Foundation (Grant 2020M680013). F.Y. thanks the US NSF for funding support (Grant AGS1550816). We acknowledge the National Supercomputing Center in Shenzhen for providing the computational resources and Turbomole.

1. R. Zhang, A. Khalizov, L. Wang, M. Hu, W. Xu, Nucleation and growth of nanoparticles in the atmosphere. *Chem. Rev.* **112**, 1957–2011 (2012).
2. C. Kuang, P. H. McMurry, A. V. McCormick, Determination of cloud condensation nuclei production from measured new particle formation events. *Geophys. Res. Lett.* **36**, 1–5 (2009).
3. M. Sipilä *et al.*, The role of sulfuric acid in atmospheric nucleation. *Science* **327**, 1243–1246 (2010).
4. J. Kirkby *et al.*, Role of sulphuric acid, ammonia and galactic cosmic rays in atmospheric aerosol nucleation. *Nature* **476**, 429–433 (2011).
5. H. Yu, L. Ren, V. P. Kanawade, New particle formation and growth mechanisms in highly polluted environments. *Curr. Pollut. Rep.* **3**, 245–253 (2017).
6. S. H. Lee *et al.*, New particle formation in the atmosphere: From molecular clusters to global climate. *J. Geophys. Res. Atmos.* **124**, 7098–7146 (2019).
7. R. Cai *et al.*, Sulfuric acid—amine nucleation in urban Beijing. *Atmos. Chem. Phys.* **21**, 2457–2468 (2021).
8. N. Zhao, Q. Zhang, W. Wang, Atmospheric oxidation of phenanthrene initiated by OH radicals in the presence of O_2 and NO_x—A theoretical study. *Sci. Total Environ.* **563-564**, 1008–1015 (2016).
9. K. Acker, D. Möller, R. Auel, W. Wieprecht, D. Kalaß, Concentrations of nitrous acid, nitric acid, nitrite and nitrate in the gas and aerosol phase at a site in the emission zone during ESCOMPTE 2001 experiment. *Atmos. Res.* **74**, 507–524 (2005).
10. R. Zhang *et al.*, Secondary inorganic aerosols formation during haze episodes at an urban site in Beijing, China. *Atmos. Environ.* **177**, 275–282 (2018).
11. J. Ding *et al.*, Aerosol pH and its driving factors in Beijing. *Atmos. Chem. Phys.* **19**, 7939–7954 (2019).
12. M. Wang *et al.*, Rapid growth of new atmospheric particles by nitric acid and ammonia condensation. *Nature* **581**, 184–189 (2020).
13. L. Liu *et al.*, The role of nitric acid in atmospheric new particle formation. *Phys. Chem. Chem. Phys.* **20**, 17406–17414 (2018).
14. L. Yao *et al.*, Atmospheric new particle formation from sulfuric acid and amines in a Chinese megacity. *Science* **361**, 278–281 (2018).
15. J. Mao *et al.*, High–resolution modeling of gaseous methylamines over a polluted region in China: Source–dependent emissions and implications of spatial variations. *Atmos. Chem. Phys.* **18**, 7933–7950 (2018).
16. M. J. McGrath *et al.*, Atmospheric Cluster Dynamics Code: A flexible method for solution of the birth–death equations. *Atmos. Chem. Phys.* **12**, 2345–2355 (2012).
17. T. Olenius, O. Kupiainen-Määttä, I. K. Ortega, T. Kurtén, H. Vehkamäki, Free energy barrier in the growth of sulfuric acid-ammonia and sulfuric acid-dimethylamine clusters. *J. Chem. Phys.* **139**, 084312 (2013).
18. R. F. W. Bader, *Atoms in Molecules: A Quantum Theory* (Oxford Science Publications, 1990).
19. H. L. Schmider, A. D. Becke, Chemical content of the kinetic energy density. *J. Mol. Struct. THEOCHEM* **527**, 51–61 (2000).

20. I. J. Kurnig, S. Scheiner, Ab Initio investigation of the structure of hydrogen halide–amine complexes in the gas phase and in a polarizable medium. *Int. J. Quantum Chem.* **14**, 47–56 (1987).
21. S. W. Hunt, K. J. Higgins, M. B. Craddock, C. S. Brauer, K. R. Leopold, Influence of a polar near-neighbor on incipient proton transfer in a strongly hydrogen bonded complex. *J. Am. Chem. Soc.* **125**, 13850–13860 (2003).
22. POWER Data Access Viewer, Version 2.0.0. https://power.larc.nasa.gov/data-access-viewer/. Accessed 29 May 2020.
23. F. Yu, G. Luo, Modeling of gaseous methylamines in the global atmosphere: Impacts of oxidation and aerosol uptake. *Atmos. Chem. Phys.* **14**, 12455–12464 (2014).
24. H. Vehkamäki *et al*., Atmospheric particle formation events at Värriö measurement station in Finnish Lapland 1998–2002. *Atmos. Chem. Phys.* **4**, 2015–2023 (2004).
25. M. Komppula *et al*., New particle formation in air mass transported between two measurement sites in Northern Finland. *Atmos. Chem. Phys.* **6**, 2811–2824 (2006).
26. D. Spracklen *et al*., The contribution of boundary layer nucleation events to total particle concentrations on regional and global scales. *Atmos. Chem. Phys.* **6**, 5631–5648 (2006).
27. F. Yu *et al*., Spatial distributions of particle number concentrations in the global troposphere: Simulations, observations, and implications for nucleation mechanisms. *J. Geophys. Res.* **115**, D17205 (2010).
28. J. Zhang, M. Dolg, ABCluster: The artificial bee colony algorithm for cluster global optimization. *Phys. Chem. Chem. Phys.* **17**, 24173–24181 (2015).
29. J. Zhang, M. Dolg, Global optimization of clusters of rigid molecules using the artificial bee colony algorithm. *Phys. Chem. Chem. Phys.* **18**, 3003–3010 (2016).
30. K. Vanommeslaeghe *et al*., CHARMM general force field: A force field for drug-like molecules compatible with the CHARMM all-atom additive biological force fields. *J. Comput. Chem.* **31**, 671–690 (2010).
31. J. J. P. Stewart, Optimization of parameters for semiempirical methods V: Modification of NDDO approximations and application to 70 elements. *J. Mol. Model.* **13**, 1173–1213 (2007).
32. MOPAC, Version 2016. http://OpenMOPAC.net. Accessed 12 May 2020.
33. Y. Zhao, D. G. Truhlar, The M06 suite of density functionals for main group thermochemistry, thermochemical kinetics, noncovalent interactions, excited states, and transition elements: Two new functionals and systematic testing of four M06–class functionals and 12 other functionals. *Theor. Chem. Acc.* **120**, 215–241 (2008).
34. Y. Zhao, D. G. Truhlar, Applications and validations of the minnenesota density functionals. *Chem. Phys. Lett.* **502**, 1–13 (2011).
35. M. J. Frisch, J. A. Pople, J. S. Binkley, Self–consistent molecular orbital methods 25. supplementary functions for Gaussian basis sets. *Chem. Phys. Lett.* **80**, 3265–3269 (1984).
36. N. Bork, J. Elm, T. Olenius, H. Vehkamäki, Methane sulfonic acid–enhanced formation of molecular clusters of sulfuric acid and dimethyl amine. *Atmos. Chem. Phys.* **14**, 12023–12030 (2014).
37. J. Elm, M. Bilde, K. V. Mikkelsen, Assessment of density functional theory in predicting structures and free energies of reaction of atmospheric prenucleation clusters. *J. Chem. Theory Comput.* **8**, 2071–2077 (2012).
38. A. B. Nadykto, F. Yu, J. Herb, Ammonia in positively charged pre–nucleation clusters: A quantum–chemical study and atmospheric implications. *Atmos. Chem. Phys.* **9**, 4031–4038 (2009).
39. A. B. Nadykto, F. Yu, M. V. Jakovleva, J. Herb, Y. Xu, Amines in the Earth's atmosphere: A density functional theory study of the thermochemistry of pre-nucleation clusters. *Entropy* **13**, 554–569 (2011).
40. J. Elm, M. Bilde, K. V. Mikkelsen, Assessment of binding energies of atmospherically relevant clusters. *Phys. Chem. Chem. Phys.* **15**, 16442–16445 (2013).
41. M. J. Frisch *et al*., *Gaussian 09, Revision A.1* (Gaussian Inc., 2009).
42. N. Myllys, J. Elm, R. Halonen, T. Kurtén, H. Vehkamäki, Coupled cluster evaluation of the stability of atmospheric acid–base clusters with up to 10 molecules. *J. Phys. Chem. A* **120**, 621–630 (2016).
43. G. Schmitz, J. Elm, Assessment of the DLPNO binding energies of strongly noncovalent bonded atmospheric molecular clusters. *ACS Omega* **5**, 7601–7612 (2020).
44. C. Riplinger, F. Neese, An efficient and near linear scaling pair natural orbital based local coupled cluster method. *J. Chem. Phys.* **138**, 034106 (2013).
45. C. Riplinger, B. Sandhoefer, A. Hansen, F. Neese, Natural triple excitations in local coupled cluster calculations with pair natural orbitals. *J. Chem. Phys.* **139**, 134101 (2013).
46. J. Dunning, K. A. Peterson, A. K. Wilson, Gaussian basis sets for use in correlated molecular calculations. X. The atoms aluminum through argon revisited. *J. Chem. Phys.* **114**, 9244–9253 (2001).
47. F. Neese, The ORCA program system. *Wiley Interdiscip. Rev. Comput. Mol. Sci.* **2**, 73–78 (2012).
48. L. F. Shampine, M. W. Reichelt, The MATLAB ODE Suite. *J. Am. Chem. Soc.* **18**, 1–22 (1997).
49. C. Hättig, F. Weigend, CC2 excitation energy calculations on large molecules using the resolution of the identity approximation. *J. Chem. Phys.* **113**, 5154–5161 (2000).
50. Y. Lu *et al*., Atmospheric sulfuric acid-dimethylamine nucleation enhanced by trifluoroacetic acid. *Geophys. Res. Lett.* **47**, e2019GL085627 (2020).
51. J. Almeida *et al*., Molecular understanding of sulphuric acid-amine particle nucleation in the atmosphere. *Nature* **502**, 359–363 (2013).
52. A. Kürten *et al*., New particle formation in the sulfuric acid–dimethylamine–water system: Reevaluation of CLOUD chamber measurements and comparison to an aerosol nucleation and growth model. *Atmos. Chem. Phys.* **18**, 845–863 (2018).
53. A. Kürten, L. Rondo, S. Ehrhart, J. Curtius, Calibration of a chemical ionization mass spectrometer for the measurement of gaseous sulfuric acid. *J. Phys. Chem. A* **116**, 6375–6386 (2012).
54. J. Zheng *et al*., Development of a new corona discharge based ion source for high resolution time-of-flight chemical ionization mass spectrometer to measure gaseous H_2SO_4 and aerosol sulfate. *Atmos. Environ.* **119**, 167–173 (2015).
55. S. S. Brown *et al*., Variability in nocturnal nitrogen oxide processing and its role in regional air quality. *Science* **311**, 67–70 (2006).
56. K. Mezuman, S. E. Bauer, K. Tsigaridis, Evaluating secondary inorganic aerosols in three dimensions. *Atmos. Chem. Phys.* **16**, 10651–10669 (2016).
57. T. D. Fairlie *et al*., Impact of mineral dust on nitrate, sulfate, and ozone in transpacific Asian pollution plumes. *Atmos. Chem. Phys.* **20**, 3999–4012 (2010).
58. C. H. Song, G. R. Carmichael, A three-dimensional modelling investigation of the evolution processes of dust and seasalt particles in east Asia. *J. Geophys. Res.* **106**, 18131–18154 (2001).
59. D. V. Vayenas, S. Takahama, C. I. Davidson, S. N. Pandis, Simulation of the thermodynamics and removal processes in the sulfate-ammonia-nitric acid system during winter: Implications for PM2.5 control strategies. *J. Geophys. Res. Atmos.* **110**, D07S14 (2005).
60. M. Kumar, J. Zhong, X. C. Zeng, J. S. Francisco, Reaction of criegee intermediate with nitric acid at the air–water interface. *J. Am. Chem. Soc.* **140**, 4913–4921 (2018).
61. S. Aloiso, J. S. Francisco, Structure and energetics of hydrogen bonded HO_x–HNO_3 complexes. *J. Phys. Chem. A* **103**, 6049–6053 (1999).
62. R. J. Weber *et al*., Measured atmospheric new particle formation rates: Implications for nucleation mechanisms. *Chem. Eng. Commun.* **151**, 53–64 (1996).
63. P. Paasonen *et al*., On the formation of sulphuric acid–amine clusters in varying atmospheric conditions and its influence on atmospheric new particle formation. *Atmos. Chem. Phys.* **12**, 9113–9133 (2012).
64. H. B. Xie *et al*., Atmospheric fate of monoethanolamine: Enhancing new particle formation of sulfuric acid as an important removal process. *Environ. Sci. Technol.* **51**, 8422–8431 (2017).
65. L. Liu, F. Yu, K. Tu, Z. Yang, X. Zhang, Influence of atmospheric conditions on the role of trifluoroacetic acid in atmospheric sulfuric acid–dimethylamine nucleation. *Atmos. Chem. Phys.* **21**, 6221–6230 (2021).